SAN096-2494C
CONF-9610170--5 SAND--96-2494C

Penetration into Limestone Targets with Ogive-Nose Steel Projectiles

D. J. Frew[1], M. J. Forrestal[2], S. J. Hanchak[3], and M. L. Green[1]
[1]Waterways Experiment Station, Vicksburg, MS 39180-6199
[2]Sandia National Laboratories, Albuquerque, NM 87185-0303
[3]University of Dayton Research Institute, Dayton, OH 45469-0182

Abstract

We conducted depth of penetration experiments into limestone targets with 3.0 caliber-radius-head, 4340 Rc 45 steel projectiles. Powder guns launched two projectiles with length-to-diameter ratios of ten to striking velocities between 0.4 and 1.5 km/s. Projectiles had diameters and masses of 12.7 mm, 0.117 kg and 25.4 mm, 0.610 kg. Based on data sets with these two projectile scales, we proposed an empirical penetration equation that described the target by its density and an empirical strength constant determined from penetration depth versus striking velocity data.

Introduction

In this study, we conducted laboratory-scale penetration experiments with limestone targets and 4340 Rc 45 steel, ogive-nose projectiles. Post-test observations showed a nearly conical entry crater on the impact surface with an approximate depth of two projectile diameters followed by a circular tunnel with nearly the projectile diameter. We previously found the same observations for studies with concrete targets (Forrestal, Altman, Cargile, and Hanchak, 1994, and Forrestal, Frew, Hanchak, and Brar, 1996). For concrete targets, we developed a penetration equation that depends on the projectile geometry and mass, the target density, unconfined compressive strength, and a dimensionless empirical constant that depends only on the unconfined compressive strength of the target. The dimensionless empirical constant is found from depth of penetration versus striking velocity data. Since the empirical constant depends only on the unconfined compressive strength of the target, we were able to then predict with reasonable accuracy the depth of penetration for larger scale projectiles.

The unconfined compressive strengths for the three batches of limestone targets used in this study were quarried* from nearby sites and varied from 43–64 MPa, so we were not able to use unconfined strength in our penetration equation for limestone targets. However, when we conducted triaxial compressions tests at or just beyond the ductile transition with 50 MPa confining pressure, the shear strength was nearly the same for the three target batches (Ashby and Sammis, 1990, and Fossum, Senseny, Pfeifle, and Mellegard, 1995). Thus, our penetration equation for limestone targets contains an empirical strength constant, R (Pa), that we determine from penetration data. We speculate that this penetration equation will be reasonably accurate for larger scale projectiles, but data from field tests with larger projectiles must be obtained to confirm our speculation.

* Elliot Stone Company, Bedford, Indiana.

This work was supported by the United States Department of Energy under Contract DE-AC04-94AL85000.
Sandia is a multiprogram laboratory operated by Sandia Corporation, a Lockheed Martin Company, for the United States Department of Energy.

DISCLAIMER

Experiments

We conducted depth of penetration experiments into limestone targets with the two projectiles dimensioned in Fig. 1. Both projectiles were machined from 4340 Rc 45 steel and had 3.0 caliber-radius-head nose shapes and a total length-to-diameter ratio of ten.

The limestone targets were quarried and cut by the Elliot Stone Company of Bedford, Indiana. We obtained the targets in three batches from nearby sites. Some physical properties and the unconfined compressive strengths are given in Table 1. Data from triaxial material tests with 50 MPa confining pressure are presented in Fig. 2. As previously discussed, there are large differences in the unconfined strengths, but the confined strengths with 50 MPa confining pressure are nearly equal.

The 12.7-mm-diameter, 0.117 kg projectiles.

The 4340 Rc 45 steel rod projectile is dimensioned in Fig. 1a and penetration data are given in Table 2. This set of experiments used the limestone targets listed as batch 1 in Table 1 and Fig. 2. The target impact surface was 0.51-m-square and target lengths are given in Table 2. The sides and bottom of the targets were surrounded by 0.10-m-thick concrete placed between a steel form and the limestone targets.

A 30-mm-diameter powder gun launched the projectiles to the striking velocities recorded in Table 2. Two additional experiments were conducted at Vs = 1,600 m/s, but we obtained curved trajectories. One projectile came to rest in the surrounding concrete and the other exited the target.

The 25.4-mm-diameter, 0.610 kg projectiles.

The 4340 Rc 45 steel projectile is dimensioned in Fig. 1b and the penetration data are given in Table 3. This set of experiments used the limestone targets listed as batches 2 and 3 in Table 1 and Fig. 3. The target impact surface was 1.02-m-square and target lengths are given in Table 3. The sides and bottom of the targets were surrounded by 0.051-m-thick concrete placed between a steel form and the limestone targets. Targets for shot numbers RPSL-12 and RPSL-10 in Table 3 used targets designated as batch 3 and the remaining experiments used targets designated as batch 2.

An 83-mm-diameter powder gun launched the projectiles to the striking velocities recorded in Table 3. One additional experiment was conducted at Vs = 1,300 m/s, but the rear end of the shank fractured in the penetration tunnel.

Penetration Model

As previously discussed, our penetration model for limestone targets does not use unconfined compressive strength f_c'. For limestone targets, we replace Sf_c' in our

concrete penetration model (Forrestal, Altman, Cargile, and Hanchak, 1994) with R. Thus, final penetration depth is given by

$$P = \frac{m}{2\pi a^2 \rho N} \ln\left(1 + \frac{N\rho V_1^2}{\mathrm{R}}\right) + 4a, \quad P > 4a \tag{1a}$$

$$N = \frac{8\psi - 1}{24\psi^2} \quad , \quad V_1^2 = \frac{mV_s^2 - 4\pi a^3 \mathrm{R}}{m + 4\pi a^3 N\rho} \tag{1b}$$

where the projectile has mass m, shank diameter $2a$, and nose shape with caliber-radius-head ψ. The target is described by density ρ and an empirical strength constant R determined from penetration depth versus striking velocity data given by

$$\mathrm{R} = \frac{N\rho V_s^2}{\left(1 + \dfrac{4\pi a^3 N\rho}{m}\right)\exp\left[\dfrac{2\pi a^2 (P - 4a) N\rho}{m}\right] - 1} \, . \tag{2}$$

For each experiment with a particular projectile, we calculate a value of R. Values of R are recorded in Tables 2 and 3. For the data in Tables 2 and 3, the average values of R are 0.705 GPa and 0.790 GPa. Since values of R depend only on the target, we can predict penetration depth for field tests conducted with larger scale projectiles.

Results and Discussion

Figure 3 shows penetration depth versus striking velocity data for the 12.7-mm-diameter projectile and a prediction from equation (1). In equation (1) we use the average value of R = 0.790 GPa. Figure 4 presents penetration data for the 25.4-mm-diameter projectile and predictions from equation (1). The solid line in Fig. 4 uses the average value of R = 0.705 GPa calculated from values given in Table 3, whereas the dashed line uses R = 0.790 calculated from the 12.7-mm-diameter data given in Table 2.

As previously discussed, we obtained three batches of limestone targets quarried from sites close to each other, but Table 1 and Fig. 3 show differences in the material physical and strength properties. In addition, Fig. 4 shows slight differences in penetration data for the different batches of limestone targets. Our predictive method requires penetration data to obtain the strength constant R, which is independent of the projectile parameters. So, from laboratory-scale experiments we obtain R and can predict or estimate depth of penetration versus striking velocity for much more expensive field tests with larger scale projectiles. Our method has worked well for concrete targets, but field tests into limestone targets have not yet been conducted.

Acknowledgment

This work was supported by Sandia National Laboratories Joint DoD/DOE Penetration Technology Project and the Defense Special Weapons Agency.

References

1. Ashby, M. F., and Sammis, C. G., 1990, "The Damage Mechanics of Brittle Solids in Compression," *Pure and Applied Geophysics*, Vol. 133, No. 3, pp. 489–521.

2. Forrestal, M. J., Altman, B. S., Cargile, J. D., and Hanchak, S. J., 1994, "An Empirical Equation for Penetration Depth of Ogive-Nose Projectiles into Concrete Targets," *International Journal of Impact Engineering*, Vol. 15, No. 4, pp. 395–405.

3. Forrestal, M. J., Frew, D. J., Hanchak, S. J., and Brar, N. S., "Penetration of Grout and Concrete Targets with Ogive-Nose Steel Projectiles," 1996, *International Journal of Impact Engineering*, Vol. 18, No. 5, pp. 465–476.

4. Fossum, A. F., Senseny, P. E., Pfeifle, T. W., and Mellegard, K. D., 1995, "Experimental Determination of Probability Distributions for Parameters of a Salem Limestone Cap Plasticity Model," *Mechanics of Materials*, pp. 119–137.

Table 1. Limestone target material properties.

Batch	Density ρ (Mg/m^3)	Porosity η (%)	Unconfined Strength f_c' (MPa)
1	2.32	14.4	64
2	2.28	15.9	43
3	2.27	16.3	56

Table 2. Penetration data for the 12.7-mm-diameter, 0.117 kg projectiles. For pitch and yaw, D=down, U=up, R=right, L=left.

Shot Number	Target Length (m)	Striking Velocity (m/s)	Pitch Yaw (degrees)	Penetration Depth (m)	Projectile Mass Loss (percent)	R (GPa)
1-0370	0.61	459	1.9D.3.0L	0.141	0.16	0.74
1-0371	0.61	608	1.0U,1.0R	0.232	0.24	0.722
1-0372	0.91	853	0,0	0.362	0.96	0.881
1-0377	0.91	956	0,0.3L	0.523	1.29	0.722
1-0373	0.91	1134	1.0U,1.9R	0.562	2.59	0.937
1-0376	1.22	1269	0,0	0.812	3.87	0.748
1-0375	1.22	1404	0,0.7R	0.924	5.25	0.783
1-0374	1.22	1502	0.7U,0	1.017	5.90	0.791

Table 3. Penetration data for the 25.4-mm-diameter, 0.610 kg projectiles. For pitch and yaw, D=down, U=up, R=right, L=left.

Shot Number	Target Length (m)	Striking Velocity (m/s)	Pitch Yaw (degrees)	Penetration Depth (m)	R (GPa)
RPSL-6	1.38	560		0.30	0.651
RPSL-2	1.38	731	1.1D,2.0U	0.42	0.755
RPSL-1	1.38	793		0.53	0.677
RPSL-4	1.38	939		0.73	0.652
RPSL-3	1.38	984		0.74	0.706
RPSL-12	1.52	1098	2.1U,2.5R	0.79	0.812
RPSL-10	1.52	1184	1.8U,0.3L	1.03	0.683

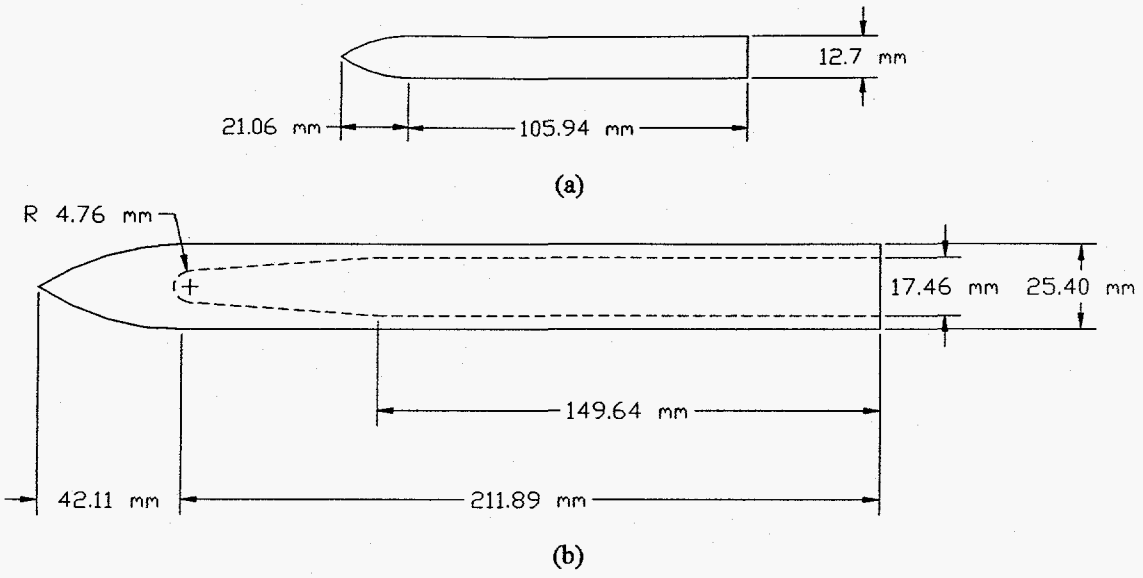

Figure 1. Projectile Geometries

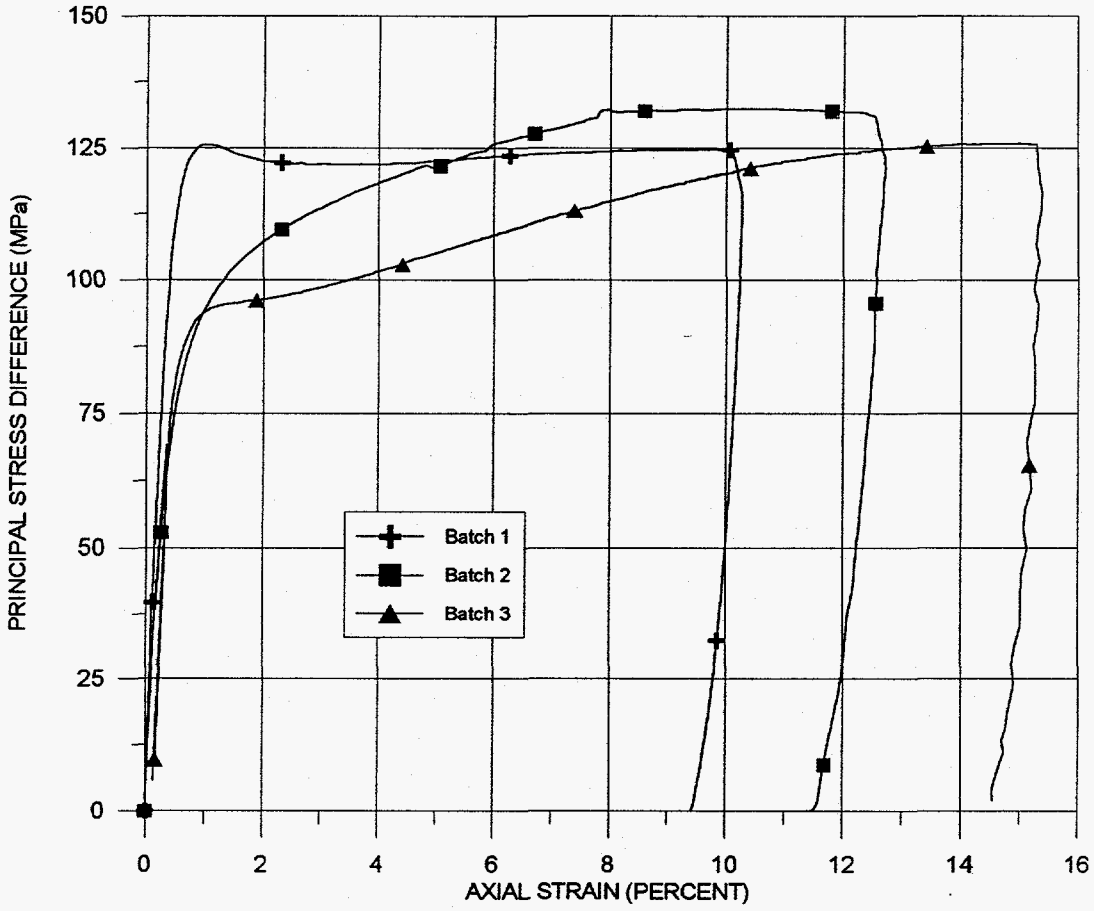

Figure 2 Triaxial data for 50 MPa confining pressure

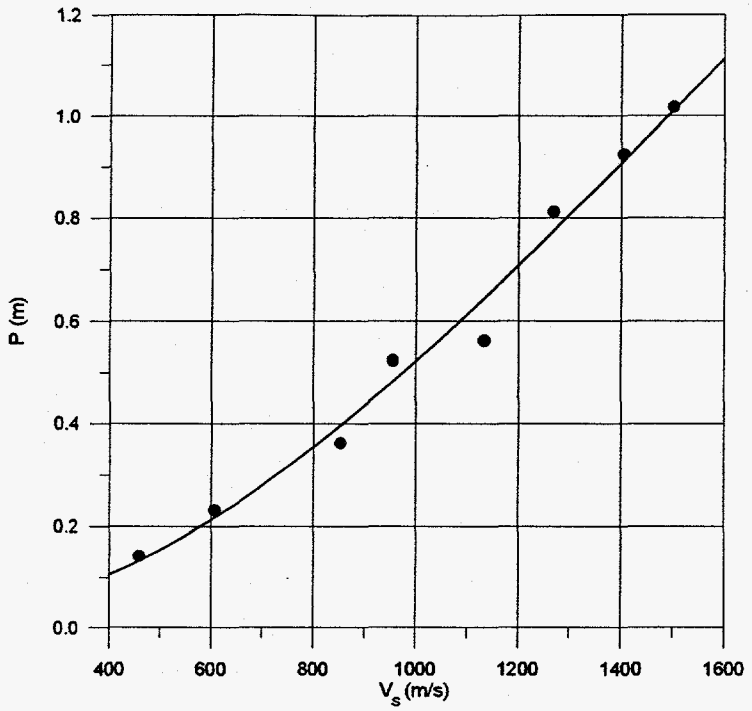

Figure 3. Data and model predictions for the 12.7-mm-diameter projectiles

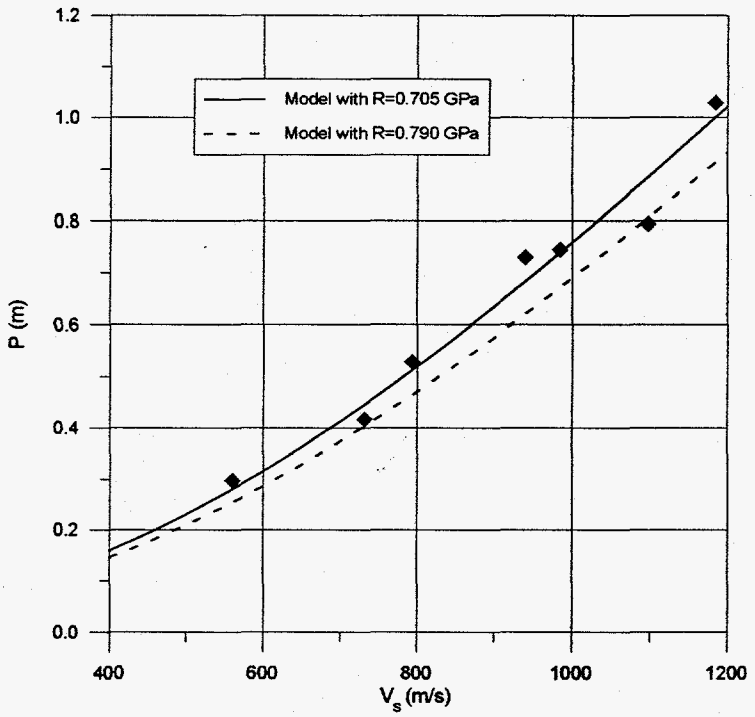

Figure 4 Data and model predictions for the 25.4-mm-diameter projectiles